Weak antilocalization in HgTe double wells with massive Dirac fermions

© N.M. Kawahala[1], G.M. Gusev[1], E.B. Olshanetsky[2,3], F.G.G. Hernandez[1], N.N. Mikhailov[2], S.A. Dvoretsky[2]

[1] Instituto de Física da Universidade de São Paulo,
135960-170, São Paulo, SP, Brazil
[2] Rzhanov Institute of Semiconductor Physics, Siberian Branch, Russian Academy of Sciences,
630090 Novosibirsk, Russia
[3] Novosibirsk State Technical University NETI,
630073 Novosibirsk, Russia

E-mail: eolsh@isp.nsc.ru

Received April 8, 2024
Revised June 5, 2024
Accepted June 5, 2024

The HgTe double quantum well is a two-dimensional topological insulator in which the bulk carriers are massive Dirac fermions with a vanishingly small Berry curvature. Accordingly, the nature of quantum corrections to the conductivity in such a system should be determined by the presence of two factors: a near-zero Berry phase and spin-orbit scattering. In particular, the vanishing Berry curvature in the HgTe double quantum well should, according to the theory, lead to the observation of negative magnetoresistance, while in a single HgTe quantum well with massless Dirac fermions and a non-zero Berry phase, the theory always predicts antilocalization corrections to the conductivity (positive magnetoresistance) regardless of the strength of the spin-orbit interaction. In the present work, contrary to expectations, similar antilocalization corrections to the conductivity of positive magnetoresistance were also found in the double HgTe quantum well, which indicates the dominance of the spin-orbit relaxation mechanism in quantum transport, leading to weak antilocalization. Thus, the results of our study of interference corrections to the conductivity in the system of massive Dirac fermions indicate that the physics of localization in two-dimensional topological insulators is determined by the competition of such factors as the spin texture, the mass of the quasiparticle, and the intensity of spin-orbit scattering.

Keywords: two-dimensional topological insulator, double quantum well, magnetoresistance, weak localization.

DOI: 10.61011/SC.2024.05.59174.6232

1. Introduction

It's commonly believed that in a disordered two-dimensional (2D) system the charge carriers are always localized irrespective of the disorder force [1]. The main reason for this is quantum interference which at small disorder leads to weak-localization corrections to conductivity which is a precursor for a strong localization. The issue of versatility of weak localization (WL) and weak anti-localization (WAL) concepts for 2D fermion systems, in general, still remains unclear, including topological insulators with massless or massive Dirac fermions that have been discovered for the last 15 years [2–6].

Thus, the 3D topological insulators (3DTI) are characterized by availability of a band gap in the 3D spectrum and gapless conducting surface states. These states, in terms of topology, are protected against back scattering ([6,7]) because back scattering cannot occur without simultaneous spin flip (topological states with an opposite pulse have an opposite spin). At the same time in such system the interference between the trajectories propagating clockwise and counterclockwise turns out to be destructive because of Dirac fermions system-specific Berry phase mechanism which leads to the weak anti-localization behavior of the surface states [8–10]. Transition from WL to WAL is expected to occur in 3DTI films depending on the film thickness. This is because hybridization of upper and lower surface states results in manifestation of Dirac mass fermions and Berry phase deviation from π [11]. Thus, the sign of interference correction to conductivity depends on the mass of the quasi-particle: for zero mass or at its small values correction corresponds to WAL, which is peculiar to the topological insulators, and with large masses the correction corresponds to WL, as in conventional mass fermion system. It should be, however, stressed that the required mass variation range is quite extensive which makes it unlikely to get the adjusted topological transition WL-WAL on the base of 3DTI films [12,13].

Another version of 2D Dirac fermions system is a quantum well (QW) on the base of HgTe. When the width of HgTe d well is close to its critical value, $d \sim d_c \approx 6.3$ nm, the spectrum becomes gapless and at low levels of energy looks like Dirac spectrum for the massless fermions $\varepsilon_{\pm}(k) = \pm Ak$, where k — wave vector, two signs correspond to the electron and hole bands, and A — parameter that can be obtained from effective Hamiltonian for a narrow symmetrical QW HgTe [3]. In quantum wells with the width different from the critical one the dispersion law is written as follows:

$$\varepsilon_{\pm}(k) = Dk^2 \pm \sqrt{A^2k^2 + (M + Bk^2)^2}, \qquad (1)$$

where M, B, D — positive parameters which depend on material, at that $B > D$. Parameter M is positive at $d < d_c$ (conventional insulator) and negative at $d > d_c$ (topological insulator). At low energy values the dispersion of mass

Dirac fermions is almost parabolic, and at high energy values it is more of a linear dependence of the wave vector. Thus, the theory may predict transition from WL to WAL with growing Fermi energy provided the sample has appropriate parameters [10].

Multiple experiments in 3DTI in fact demonstrate behavior specific for WAL [14–16], however, this may be a cumulative effect caused by contributions of surface and 3D states [13]. In this sense the results from HgTe quantum wells are interpreted more unambiguously, since contribution into transport is provided only by the carriers with dispersion expressed by equation (1), irrespective of whether Fermi level being in valence band or in conduction band [17–21]. At that, despite the fact that, as mentioned above, theory [10] predicts transition from WL-like behavior to WAL with the growth of carriers concentration, the experiments in weak magnetic fields [17,21] demonstrated that there's only WAL behavior in both, normal ($d < d_c$), and inverted ($d > d_c$) band spectrum.

The double quantum wells (DQW) represent a typical example of a two-layer system, where two QWs are separated by a tunnel-transparent barrier with a thickness of t (Figure 1, *a*). Due to additional binary degree of freedom because of possible tunneling effect between the layers the phase portrait becomes quite diverse and energy spectrum has some singularities [22–24]. In particular, Dirac fermions (DF) become massive and the spectrum is delineated by the following dispersion:

$$\varepsilon_{\pm}(k) = Dk^2 \pm k^2\sqrt{B^2 + A^2k^2}. \qquad (2)$$

At that parameters of DQW dispersion may greatly differ from the respective parameters used in single QW [25]. In Figure 1, *b, c* the spectra are given for two different DQWs used in our study. The calculation of DQW spectrum with the use of effective Hamiltonian 6×6 with Luttinger parameters is given in papers [26,27]. The energy spectrum of DQW looks like a spectrum of the bilayer graphene [28], because single HgTe quantum well can be described by effective Hamiltonian of BHZ model [3], which leads to a graphene-like Dirac cone in spectrum [29–31] for $d \sim d_c$. However, in contrast to the bilayer graphene, in HgTe DQW in gapless phase no any valley degeneration is observed and the numerically calculated spectrum at low energy may be described by equation (2) with appropriate parameters.

For massive Dirac fermions the Berry phase is equal to zero and, hence, in weak magnetic field the behavior corresponding to WL and characterized by positive magnetic conductance shall be observed. Thus, observation of WL in HgTe DQW with massive DF, in contrast to WAL for massless DF in single HgTe wells, could demonstrate the relationship between various mechanisms defining the nature of interference corrections to conductivity in Dirac fermions system, such as spin texture, mass of quasiparticles and spin-orbit interaction (SOI).

This paper outlines the findings from the study of a weak-field magnetic conductivity in HgTe DQW. Samples having both, gapless semi-metallic energy spectrum and a band

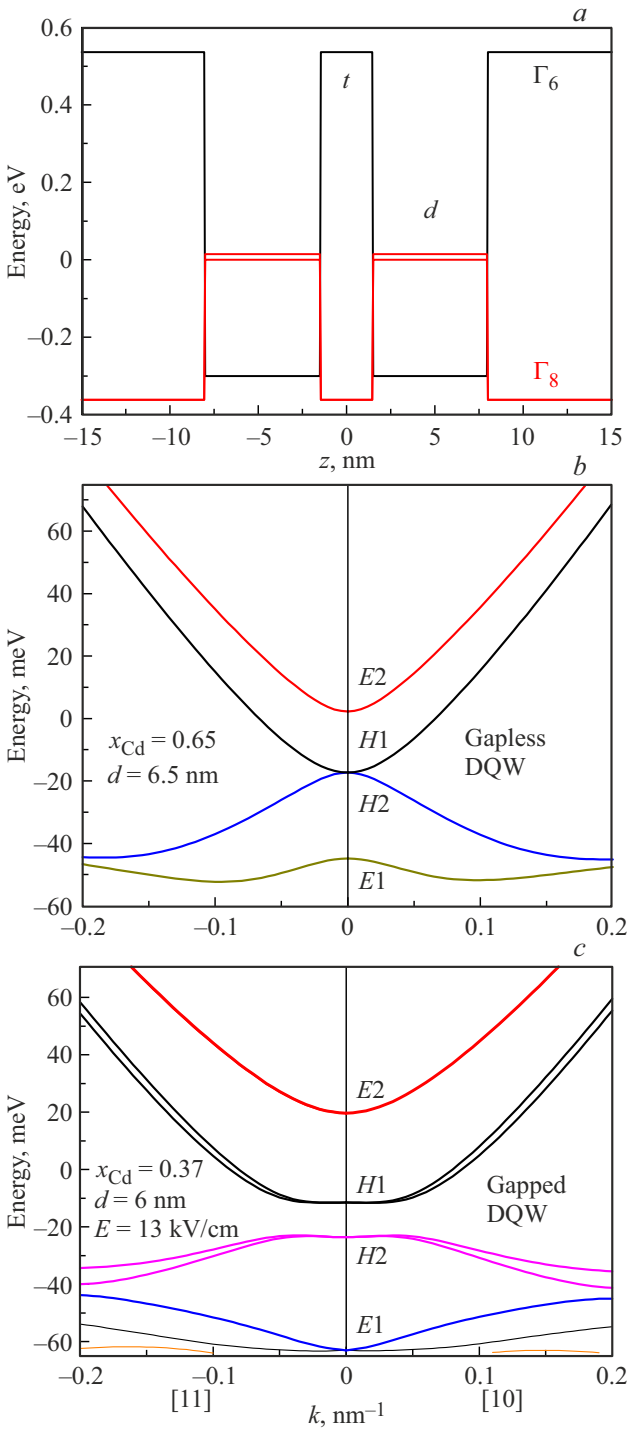

Figure 1. *a* — band spectrum profile for symmetric DQW HgTe [013] with $d = 6.5$ nm, $t = 3$ nm and Cd $x_{Cd} = 0.65$ content. *b* — energy dispersion of 2D sub-bands in two directions of the wave vector **k** in growth plane xy, $k_y = 0$ ([10]) and $k_y = k_x$ ([11]) for DQW HgTe [013] with $d = 6.5$ nm, $t = 3$ nm and Cd $x_{Cd} = 0.65$ content (gapless sample). *c* — energy dispersion of 2D sub-bands in two directions of the wave vector **k** in growth plane xy, $k_y = 0$ ([10]) and $k_y = k_x$ ([11]) for DQW HgTe [013] with $d = 6$ nm, $t = 3$ nm, with Cd $x_{Cd} = 0.37$ content and integrated electrical field $E = 13$ kV/cm (gapped sample). Edge state spectrum is not shown. (A color version of the figure is provided in the online version of the paper).

gap spectrum for 3D states were studied. In both groups of samples WAL-like behavior with negative magnetic conductivity was observed which experimentally proves the prevailing role of the spin-orbital scattering in HgTe double quantum wells.

2. Berry phase in HgTe double quantum well

To describe the low-energy states in DQW we may use a 2D Hamiltonian in the two states basis ($H1$, $H2$) obtained from the form corresponding to the four-state basis ($E1$, $H1$, $H2$, $E2$) in [22], projection of the distant states $E1$, $E2$ on the low-energy states $H1$, $H2$. It is expressed as follows:

$$\hat{H} = \begin{pmatrix} -Dk^2 + \Delta/2 - Bk^2 & Ak_-^3 \\ Ak_+^3 & -Dk^2 - \Delta/2 + Bk^2 \end{pmatrix},$$

where Δ — states splitting energy $H1$, $H2$, occurring when a mirror symmetry of DWQ is broken by the transverse electrical field. Energy reference point is taken in the middle of the gap (if Δ is non-zero) or in the contact point of bands $H1$ and $H2$ at $k = 0$ (if Δ is zero). The spectrum corresponding to $\hat{H}$, looks as follows:

$$\varepsilon_\pm(k) = -Dk^2 \pm \sqrt{(Bk^2 - \Delta/2)^2 + A^2k^6}$$

or, if $\Delta = 0$,

$$\varepsilon_\pm(k) = -Dk^2 \pm k^2\sqrt{B^2 + A^2k^2},$$

where $+$ and $-$ correspond to the states of conduction band and valence band. In case of non-zero Δ a dispersion of „Mexican hat“ type may be obtained.

Eigen states:

$$\Psi_+ = \frac{1}{\sqrt{1+\eta}}\begin{pmatrix} \sqrt{\eta}e^{-3i\varphi} \\ 1 \end{pmatrix}, \Psi_- = \frac{1}{\sqrt{1+\eta}}\begin{pmatrix} 1 \\ -\sqrt{\eta}e^{3i\varphi} \end{pmatrix},$$

where φ — angle defining the direction of the wave vector, a

$$\eta = \left[\frac{Ak^3}{Bk^2 - \Delta/2 + \sqrt{(Bk^2 - \Delta/2)^2 + A^2k^6}}\right]^2,$$

or, when $\Delta = 0$,

$$\eta = \left[\frac{Ak}{B + \sqrt{B^2 + A^2k^2}}\right]^2.$$

Berry phase for these eigen states is equal

$$\Gamma_+ = -\Gamma_- = \frac{6\pi\eta}{1+\eta}.$$

It may basically vary from 0 to 3π, but $\Gamma_+ = 3\pi$ (at $\Delta = 0$) is implemented in a quite specific case $B = 0$, which is hard to reach or, perhaps, even impossible. A is probably small compared to B, and hence, η is also small.

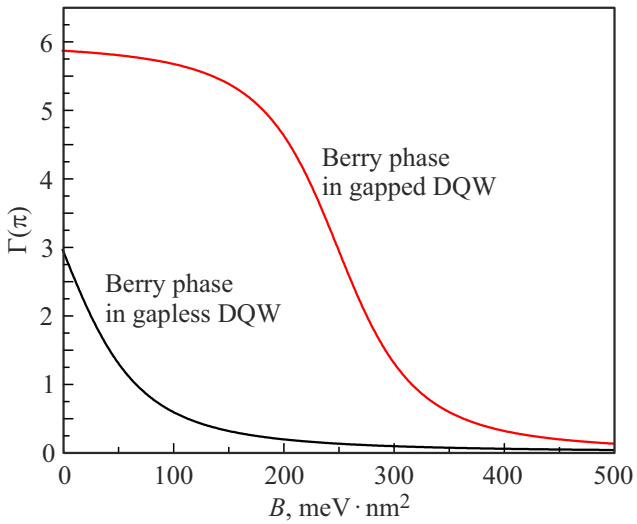

Figure 2. Berry phase versus parameter B for the gapless DQW and gapped DQW with parameters: $A = 375\,\text{meV}\cdot\text{nm}^2$, $k = 0.2\,\text{nm}^{-1}$ and $\Delta = 20\,\text{meV}$.

It is interesting to note that, although $\hat{H}$ spectrum (at $\Delta = 0$) is similar to the spectrum of bilayer graphene, $\hat{H}$ in terms of topology differs from the low-energy Hamiltonian of bilayer graphene the Berry phase of which is constant and equal 2π. Therefore, the analogy between HgTe DQW and bilayer graphene is not full.

Despite the fact that dispersion equation is defined only by three parameters D, B and A, their determination by matching the low-energy spectrum with the exact spectrum calculated by Kane model may be ambiguous. In this case it is useful to have a representation of possible range of these parameters variation.

The expression for parameters of the reduced Hamiltonian 2×2 $\hat{H}$ via parameters of Hamiltonian 4×4 from paper [22] is written as

$$D = \frac{1}{2}\left(\frac{A_1^2}{\varepsilon_{E1}} + \frac{A_2^2}{\varepsilon_{E2}}\right), \quad B = \frac{1}{2}\left(\frac{A_1^2}{\varepsilon_{E1}} - \frac{A_2^2}{\varepsilon_{E2}}\right),$$

$$A = \frac{A_1R_1}{\varepsilon_{E1}} - \frac{A_2R_2}{\varepsilon_{E2}} + \frac{S_0A_1A_2}{\varepsilon_{E1}\varepsilon_{E2}},$$

where ε_{E1} and ε_{E1} — energies of quantization of electron-like sub-bands $E1$ and $E2$ at $k = 0$.

Figure 2 shows Berry phase versus B parameter. It is seen that Γ quickly goes down at $B > 100\,\text{meV}\cdot\text{nm}^2$ in the gapless DQW and at $B > 300\,\text{meV}\cdot\text{nm}^2$ in the gapped DQW. For samples used in this paper we consider $B \approx 1000\,\text{meV}\cdot\text{nm}^2$, therefore the Berry phase in the studied double quantum wells is expected to be close to zero [22]. In this case the sign of quantum corrections to conductivity shall correspond to localization effect, i.e. it shall differ from WAL-corrections to conductivity in single QW with massless Dirac fermions [8–10].

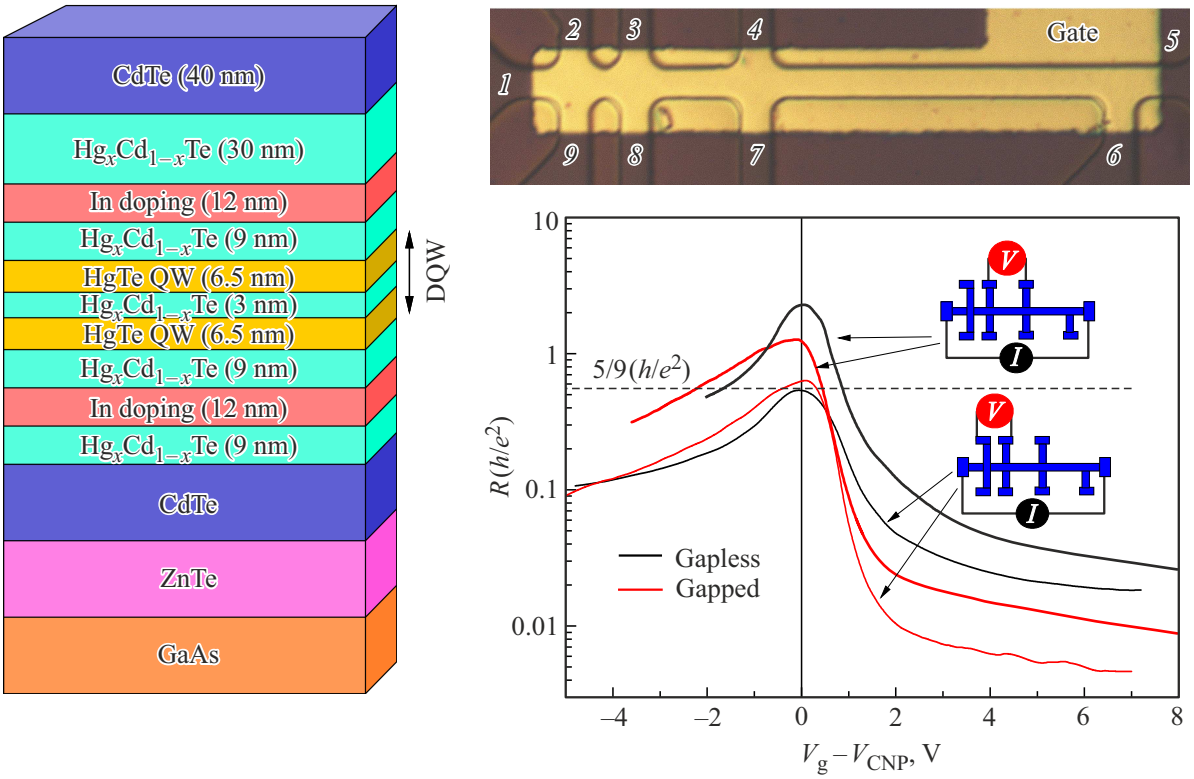

Figure 3. From the left — layer-by-layer structure diagram. From the right — top view of sample and resistance versus voltage curve on the gate for various measurement configurations and for different samples. Black lines correspond to resistance dependencies measured in gapless DQW, and red lines — in gapped DQW. The dashes designate the quantized resistance $\frac{5}{9}\,h/e^2$.

3. Samples

Structures containing HgTe quantum wells with surface orientation [013] separated by barriers $Cd_xHg_{1-x}Te$ were grown by method of molecular-beam epitaxy (MBE). A schematic representation of samples' layer-by-layer structure with a well 6.5 nm wide is given in Figure 3 (left). The use of substrates with non-singular orientations may contribute to the growth of more improved structures. Therefore, to grow the structures mainly substrates with surface orientation [013] differing from [001] by $\sim 19°$ were used. The layers thicknesses were defined by ellipsometry method during MBE growth process with an accuracy of ± 0.3 nm. The experimental samples intended for multiterminal measurements had 9 contacts and consisted of three sequential segments $W = 3.2\,\mu$m wide and having different length L (2, 8 and 32 μm) (Figure 3, top).

Ohmic contact in HgTe quantum well is fabricated similarly to its fabrication in other 2D systems, such as GaAs quantum wells: the contacts were shaped by burning in of Indium directly on the surface of contact pads. The modulation-doped HgTe/CdHgTe quantum wells are generally grown at a temperature of 180°C. Therefore, in contrast to III-V compounds, during fabrication of contacts indium was heated not so extensively. On each contact pad indium diffuses top to bottom, thus providing the ohmic contact with both quantum wells with contact resistance in the range of 10–50 kOhm. When measuring the alternating current the Y-component of impedance never exceeds 5% of the total impedance which indicates good ohmic properties of contacts.

DQW parameters $HgTe/Cd_xHg_{1-x}Te$

d, nm	t, nm	x_{Cd}	$V_{CNP}(B)$	Properties
6.5	3	0.65	−4.0	Gapless DQW
6.0	3	0.37	−2.5	Gapped DQW

A layer of dielectric SiO_2 200 nm later coated by TiAu gate was applied on the sample surface. Variation in the carriers concentration depending on gate voltage was $0.86 \cdot 10^{11}\,\text{cm}^{-2}$. Transport measurements were carried out in the temperature range from 4.2 to 20 K using conventional four-point system applying alternating current of 1–13 Hz 1–10 nA through the sample allowing to avoid heating effects. Two types of samples were studied. Table gives parameters of these samples including gate voltage corresponding to the charge neutral point (CNP) at $T = 4.2$ K. The two samples of each type were tested. Measurements on samples of the same type provided equivalent results.

4. Experimental results

Figure 3 illustrates dependencies of local resistance in zero magnetic field for samples manufactured from structures from $d = 6.5$ and 6.0 nm. In local configuration current I flows between contacts *1* and *5*, and voltage V varies between the closely located *2* and *3*, $R_L = R^{2,3}_{1,5} = V_{2,3}/I_{1,5}$ or distantly related potentiometric contacts *3* and *4*, $R_L = R^{3,4}_{1,5} = V_{3,4}/I_{1,5}$. When voltage changes on the gate due to Fermi level displacement from the conduction band into valence band the transition from electron conductivity to hole conductivity is observed. Resistance in maximum for dependencies, corresponding to the short segment has a value of $\sim 5/9(h/e^2)$, which is expected in case of a purely ballistic transport of edge states for the used resistance measurement configuration [23]. This observation is consistent with the edge state transport theory in 2D topological insulators (TI), according to which back scattering is prohibited at sufficiently low temperatures [2–6]. At the same time, peak resistance measured for the longer segment $R^{3,4}_{1,5}$ is much higher than $5/9(h/e^2)$ demonstrating the absence of ballistic nature [23]. Absence of steady edge state ballistic transport was observed by many experimental groups [32]. Many explanations of such behavior have been suggested recently [33]. A detailed discussion of existing theoretical models is out of the scope of this article.

The specifics of electron transport in DWQ structures with $d = 6.5$ and 6.0 nm has been earlier studied in [23] based on resistance temperature dependence near the charge neutrality point (CNP), which was different in these DQWs: with the growth of T the resistance (in CNP) in $d = 6.5$ nm samples grows indicating the metallic gapless type of conductivity, while resistance in $d = 6.0$ nm samples goes down at $T > 10$ K, thus indicating the presence of $\Delta = 11$ meV activation gap. Calculations of energy spectrum for asymmetric DQWs prove these conclusions and indicate that the observed gap can be generated by a transverse electrical field $E = 13$ kV/cm (Figure 1, *c*) which may appear because of an accidental deviation from the symmetrical doping of DQW that could occur during its growth by MBE method [23]. Moreover, the transport properties of 2D fermion systems in HgTe DQW in both, gapless semi-metallic phase and topological insulator phase, were also studied in perpendicular acting magnetic field [24], where multiple intersections of Landau levels of different sub-bands were observed. The dynamics of observed Landau levels intersection is well consistent with the theoretical analysis for the corresponding phases.

It should be noted that semi-metallic DQW samples and DQW samples in 2DTI phase demonstrate different behavior even with higher electrons density, away from the charge neutrality point: gapless DQWs have higher resistance and, consequently, lower mobility of the charge carriers. This may be related to the uncontrolled difference in the growth conditions. To grow the high-quality DQWs based on HgTe materials is still a challenge up to now. The observed quantized resistance near CNP is also noted to be

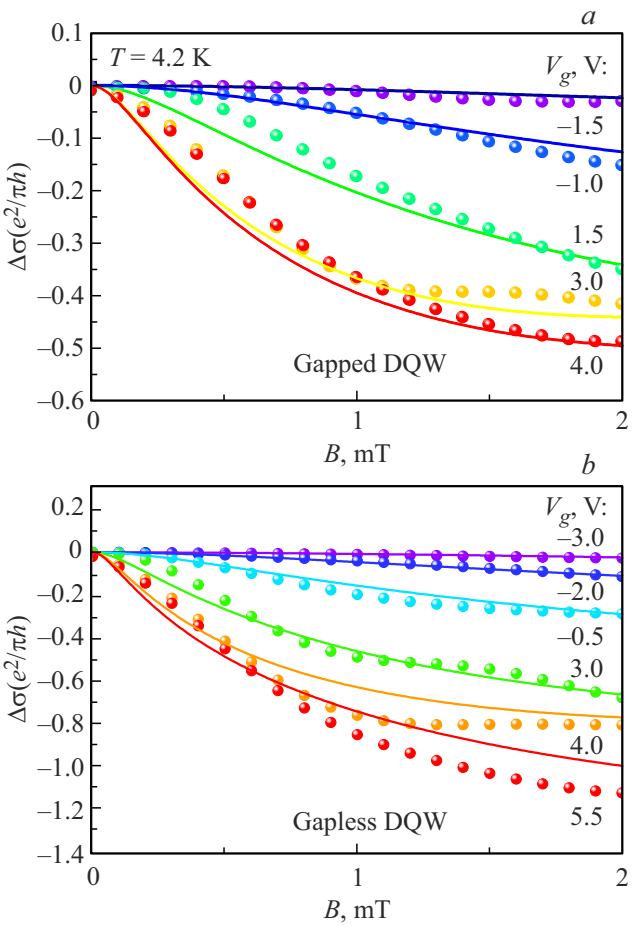

Figure 4. Experimental (round symbols) and theoretical (solid lines) dependencies of magnetic conductivity corresponding to various voltages on the gate for (*a*) DQW with a band gap and for (*b*) gapless DQW at $T = 4.2$ K.

consistent with the portrait of edge state ballistic transport in 2DTI, since resistance measured for the short segments between the potentiometric contacts doesn't depend on the sample's 3D properties. It should be stressed that the edge states exist both, in the gapless semi-metallic phase, and in the topological dielectric phase with a band gap [22,23].

Thus, the transport measurements made in the previous studies prove that the structures with $d = 6.5$ and 6.0 nm correspond to the gapless semi-metallic phase and topological insulator phase, respectively, with the energy spectra given in Figure 1, *b, c*.

From Figure 3 we may see that resistance corresponding to the electron part of the spectrum at voltages of $V_g - V_{CNP} > 1$ V becomes less $(h/5e^2)$ which complies with the weak localization conditions [34].

Figure 4, *a, b* illustrates the dependencies of magnetic conductivity $\Delta\sigma(B) = \sigma(B) - \sigma(0)$ $(\sigma = 1/\rho = \frac{L}{WR})$ as a function of magnetic field and gate voltage measured between the contacts *3* and *4* in (*a*) DQW with 2DTI and (*b*) in the gapless semi-metallic DQW. In both samples negative magnetic conductivity $(\Delta\sigma(B) < 0)$ is observed

within the entire gate voltages. A that, the amplitude of magnetic conductivity greatly increases as Fermi level is displaced from CNP to higher energies. Negative magnetic conductivity corresponds to WAL corrections to conductivity. Transition from the weak localization (WL) conductivity corrections to WAL type corrections with the change of charge carriers density was not observed in the experiment. The steady behavior corresponding to WAL instead of WL expected in DQW because of zero Berry phase (see. sect. 2) can be explained by the prevailing role of strong spin-orbit interaction in HgTe quantum well.

5. Discussion and comparison with theory

The quantitative analysis of the obtained results is based on Hikami–Larkin–Nagaoka theory modified allowing for the spin-orbit interaction [35]. The expression for magnetic conductivity is as follows

$$\Delta\sigma(B) - \Delta\sigma(0) = \frac{e^2}{2\pi^2\hbar}\left\{\psi\left(\frac{1}{2}+\frac{H_\varphi}{B}+\frac{H_{SO}}{B}\right)\right.$$
$$+\frac{1}{2}\psi\left(\frac{1}{2}+\frac{H_\varphi}{B}+\frac{2H_{SO}}{B}\right)-\frac{1}{2}\psi\left(\frac{1}{2}+\frac{H_\varphi}{B}\right)$$
$$\left.-\ln\frac{H_\varphi+H_{SO}}{B}-\frac{1}{2}\ln\frac{H_\varphi+2H_{SO}}{B}+\frac{1}{2}\ln\frac{H_\varphi}{B}\right\}, \quad (3)$$

where

$$H_\varphi = \frac{c\hbar}{4eD\tau_\varphi}, \quad H_{SO} = \frac{c\hbar}{4eD\tau_{so}},$$

τ_φ — phase coherence time, τ_{so} — spin relaxation time, $D = \frac{1}{2}v_F^2\tau_{tr}$ — diffusion constant, τ_{tr} — pulse relaxation time, ψ — digamma function.

By default we could expect that in a double quantum well the tunneling between the wells would lead to a significant change of quantum corrections to conductivity. In particular, the tunnel coupling gives to an electron an additional degree of freedom, possibility of tunneling between the layers which reduces the interference effects [36,37]. Corrections are generally defined by the ratio of phase coherence time and life time in well or tunneling time τ_t. However, in ultimate cases this theory may be simplified. For example, DQW may be considered as a structure with one quantum well, when $\tau_t \ll \tau_\varphi$, or as a system with two non-related quantum wells, when $\tau_t \gg \tau_\varphi$. In the last case the quantum corrections to conductivity represent only a sum of corrections for every individual well. Corrections to negative magnetoresistance (WL) have been studied earlier for the double quantum wells GaAs/AlGaAs [38,39].

Its' evident that adaptation to the theory of one magnetoresistance curve for simultaneous determination of several sample parameters doesn't provide the reliable results. It should be however expected that because of high difference in energies in symmetry and non-symmetry states in our DQW $\Delta_{SAS} \approx 20$ meV, the time of tunneling in it is low and by comparing the theory and experiment we may use approximation of one QW. According to our assessment, $\tau_t \sim \hbar/\Delta_{SAS} \approx 10^{-13}$ s. This time is much less than τ_φ, that, in 2D electron systems is expected to be $\sim 10^{-10}$ s [38]. Given this ratio, to describe the observed negative magnetic conductivity let's use the equation (3). Figure 4, *a, b* shows the results of comparing experimental results with AALKh theory with the use of only two adaptation parameters $L_\varphi = \sqrt{D\tau_\varphi}$ and $L_{so} = \sqrt{D\tau_{so}}$. Figure 5, *a, b* illustrates the phase and spin relaxations lengths versus electron density for both, gapless semi-metallic phase and topological insulator phase. In the same figure we may see the free path length $L_{tr} = v_F\tau_{tr}$ versus Ns, where v_F — Fermi velocity. We may see that in the available interval of electron density the following relationship between the relaxation lengths is true: $L_{tr} < L_{so} < L_\varphi$. The characteristic lengths L_{so} and L_φ become comparable only at low densities. Since $L_{tr} < L_\varphi$, we may apply diffusion theory WAL to our samples, while in the samples with higher mobility it's often required

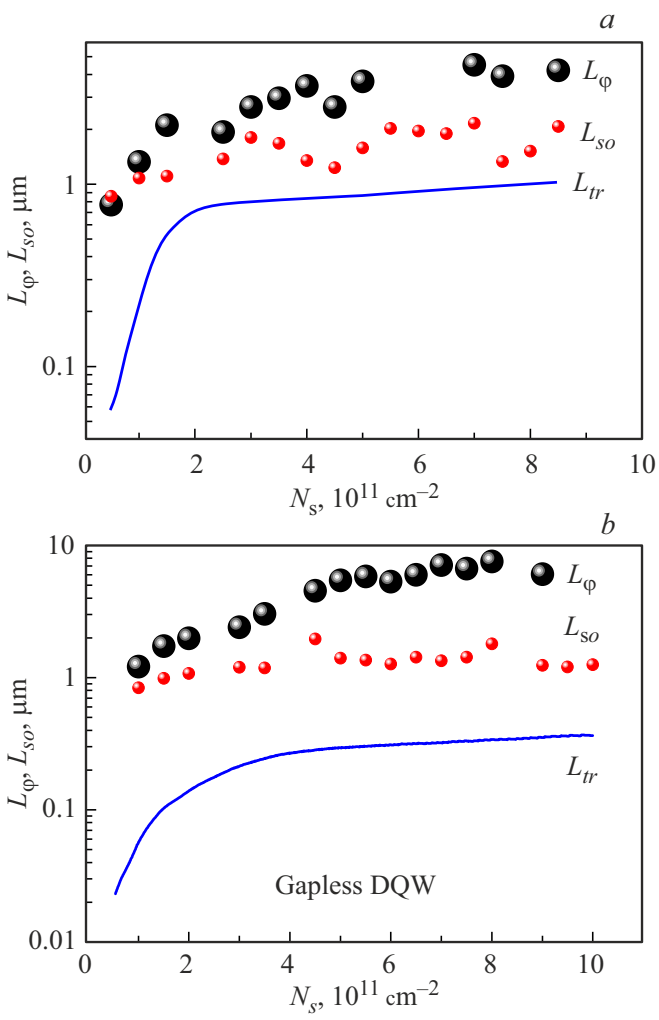

Figure 5. Experimental data L_φ (black symbols), L_{so} (red symbols) and L_{tr} (blue lines) depending on electron density for DQW with 2DTI (*a*) and for gapless DQW (*b*), $T = 4.2$ K.

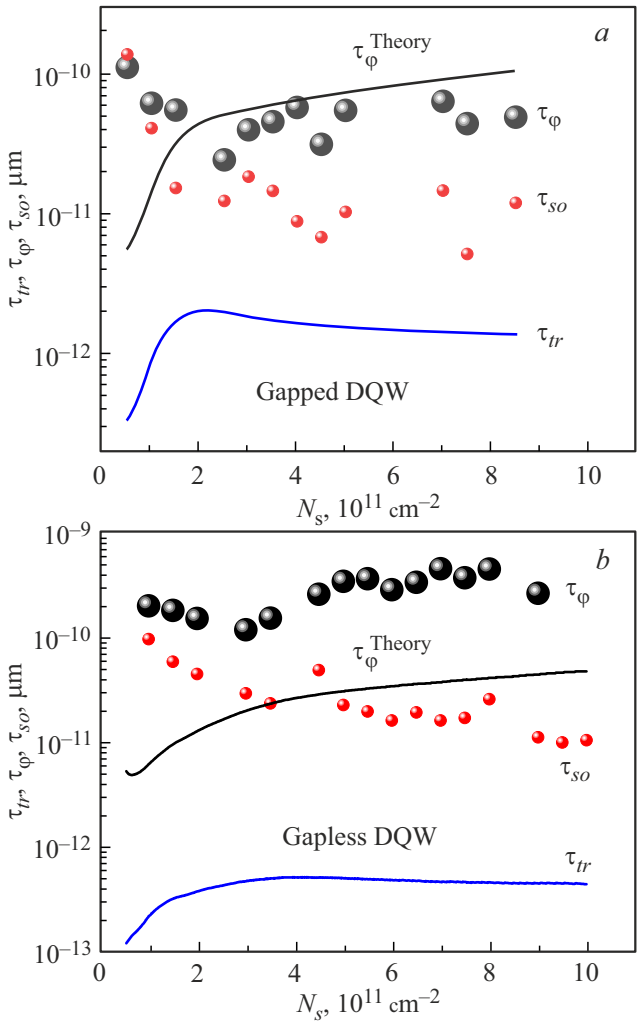

Figure 6. Experimental time of phase coherence τ_φ (black symbols) and τ_{so} (red symbols), τ_φ (black curve) calculated from equation (3), and transport relaxation time τ_{tr} (blue curve) versus electrons density for DQW with 2DTI (a) and for gapless DQW (b), $T = 4.2$ K.

to use a more common theory in ballistic and diffusion approximation [34].

Comparing the characteristic relaxation lengths obtained in the gapless DQW and in DQW with 2DTI, we find that L_{so} and L_φ have almost the same values, while L_{tr} is larger in 2DTI. Also, let's consider the characteristic relaxation times. Figure 6, *a, b* shows the relaxation times τ_φ, τ_{so} and τ_{tr} versus electronic density for both types of samples. The principal mechanism of the phase relaxation in 2D system is the electron-electron interaction in presence of disorder [34,40].

Phase relaxation time is found from the following equation:

$$\frac{1}{\tau_\varphi} = \left(\frac{k_B T}{\hbar}\right)\left(\frac{e^2/h}{\sigma}\right)\ln\left(\frac{\sigma}{e^2/h}\right), \qquad (4)$$

where k_B — Boltzmann constant. Figure 6, *a, b* shows theoretical dependencies of the phase relaxation time as a function of the carriers concentration. For a gapped DQW there's a good consistency of experimental and theoretical data, while theoretical values calculated for the gapless DQW turn to be lower than experimental data. Such discrepancy may be explained by lower charge carriers mobility in a gapless semi-metallic DQW (see Figure 3), which we attribute to additional scattering mechanism due to the sample inhomogeneity. It should be taken into account, that the studied samples have mesoscopic dimensions and their transport includes contributions from both, the edge and 3D states. At that, conductivity contribution from the edge states prevails near CNP, whereas with higher electron concentrations the decisive role plays the contribution from 3D states. The scattering between the electrons of the edge and 3D states may be sufficiently enhanced because of disorder [32]. Since WAL — is a 3D conductivity-related effect, the phase relaxation time shall be definitely defined by the 3D conductivity which may be higher here.

In 2D systems fabricated from the inversion center-free (HgTe) crystalline structures, the spin splitting of spectrum, also includes the linear Dresselhaus term, apart from the cubic Dresselhaus term in the wave vector. Moreover, in the gapped DQW because of asymmetry induced by internal electrical field, there also shall be present the k-linear Rashba splitting. However, as mentioned above the values L_{so} for both types of structures are almost equal.

It is well-known that in HgTe structures the spin-orbital interaction plays an important role [41]. In particular, it was predicted that WAL corrections remain constant within a wide concentrations range in the conduction band which is consistent with our observations. For HgTe single quantum wells in 2D topological insulator phase both effects, spin-orbit interaction and Berry phase, may result in WAL, that makes it quite difficult to define the individual contribution from each mechanism. The model offered in [41] suggests to use modified corrections WAL taking into account contributions from both effects. Since in our DQW Berry phase is equal to zero, we may expect the observed WAL effects to be defined only by SOI contribution.

6. Conclusion

For massless Dirac fermions in HgTe single quantum wells the theory predicts weak anti-localization corrections (WAL) to conductivity because of non-zero Berry phase. On the contrary, in HgTe double quantum wells because of Berry phase being close to zero we could expect to observe positive magnetic conductivity (WL). However, in this study in HgTe double quantum wells negative magnetic conductivity was observed (WAL). Observation of WAL in double quantum well structures indicates the decisive role of SOI, which, similar to non-zero Berry phase, may result in WAL. Further experimental and theoretical studies are required to differentiate between the contributions of SOI and Berry phase into conductivity corrections for massless

and massive Dirac fermions in HgTe single and double quantum wells.

Funding

The work has been funded by a grant from the Russian Science Foundation No. 23-22-00195.

Acknowledgments

G.M. Gusev expresses his thanks to O.E. Raichev for the provided theoretical analysis data.

Conflict of interest

The authors declare that they have no conflict of interest.

References

[1] P.A. Lee, T.V. Ramakrishnan. Rev. Mod. Phys., **57**, 287 (1985).
[2] C.L. Kane, E.J. Mele. Phys. Rev. Lett., **95**, 146802 (2005).
[3] B.A. Bernevig, T.L. Hughes, S.-C. Zhang. Science, **314**, 1757 (2006).
[4] M.Z. Hasan, C.L. Kane. Rev. Mod. Phys., **82**, 3045 (2010).
[5] L. Fu, C.L. Kane, E.J. Mele. Phys. Rev. Lett., **98**, 106803 (2007).
[6] X.-L. Qi, S.-C. Zhang. Rev. Mod. Phys., **83**, 1057 (2011).
[7] D.A. Kvon, Z.D. Kozlov, E.B. Olshanetsky, G.M. Gusev, N.N. Mikhailov, S.A. Dvoretsky. Physics–Uspekhi, **63** (7), 629 (2020).
[8] G. Tkachov, E.M. Hankiewicz. Phys. Rev. B, **84**, 035444 (2011).
[9] P.M. Ostrovsky, I.V. Gornyi, A.D. Mirlin. Phys. Rev. B, **86**, 125323 (2012).
[10] P.M. Ostrovsky, I.V. Gornyi, A.D. Mirlin. Phys. Rev. B, **90**, 085401 (2014).
[11] Weizhe Edward Liu, Ewelina M. Hankiewicz, Dimitrie Culcer. 2D Materials, **10**, 807 (2017).
[12] H.Z. Lu, J. Shi, S.Q. Shen. Phys. Rev. Lett., **107**, 076801 (2011).
[13] Hai-Zhou Lu, Shun-Qing Shen. Phys. Rev. B, **84**, 125138 (2011).
[14] H.T. He, G. Wang, T. Zhang, I.K. Sou, G.K.L. Wong, J.N. Wang, H.Z. Lu, S.Q. Shen, F.C. Zhang. Phys. Rev. Lett., **106**, 166805 (2011).
[15] J. Chen, X.Y. He, K.H. Wu, Z.Q. Ji, L. Lu, J.R. Shi, J.H. Smet, Y.Q. Li. Phys. Rev. B, **83**, 241304(R) (2011).
[16] Y.S. Kim, M. Brahlek, N. Bansal, E. Edrey, G.A. Kapilevich, K. Iida, M. Tanimura, Y. Horibe, S.W. Cheong,S. Oh. Phys. Rev. B, **84**, 073109 (2011).
[17] E.B. Olshanetsky, Z.D. Kvon, G.M. Gusev, N.N. Mikhailov, S.A. Dvoretsky, J.C. Portal. JETP Lett., **91**, 347 (2010).
[18] D.A. Kozlov, Z.D. Kvon, N.N. Mikhailov, S.A. Dvoretsky. JETP Lett., **96**, 730 (2013).
[19] M. Mühlbauer, A. Budewitz, B. Büttner, G. Tkachov, E.M. Hankiewicz, C. Brüne, H. Buhmann, L.W. Molenkamp. Phys. Rev. Lett., **112**, 146803 (2014).
[20] G.M. Minkov, A.V. Germanenko, O.E. Rut, A.A. Sherstobitov, S.A. Dvoretski, N.N. Mikhailov. Phys. Rev. B, **85**, 235312 (2012).
[21] G.M. Minkov, A.V. Germanenko, O.E. Rut, A.A. Sherstobitov, S.A. Dvoretski, N.N. Mikhailov. Phys. Rev. B, **88**, 045323 (2013).
[22] S.S. Krishtopenko, W. Knap, F. Teppe. Nat. Sci. Rep., **6**, 30755 (2016).
[23] G.M. Gusev, E.B. Olshanetsky, F.G.G. Hernandez, O.E. Raichev, N.N. Mikhailov, S.A. Dvoretsky. Phys. Rev. B, **101**, 241302(R) (2020).
[24] G.M. Gusev, E.B. Olshanetsky, F.G.G. Hernandez, O.E. Raichev, N.N. Mikhailov, S.A. Dvoretsky. Phys. Rev. B, **103**, 035302 (2021).
[25] P. Michetti, J.C. Budich, E.G. Novik, P. Recher. Phys. Rev. B, **85**, 125309 (2012).
[26] O.E. Raichev. Phys. Rev. B, **85**, 045310 (2012).
[27] E.G. Novik, A. Pfeuffer-Jeschke, T. Jungwirth, V. Latussek, C.R. Becker, G. Landwehr, H. Buhmann, L.W. Molenkamp. Phys. Rev. B, **72**, 035321 (2005).
[28] A.H. Castro Neto, F. Guinea, N.M.R. Peres, K.S. Novoselov, A.K. Geim. Rev. Mod. Phys., **81**, 109 (2009).
[29] B. Büttner, C.X. Liu, G. Tkachov, E.G. Novik, C. Brüne, H. Buhmann, E.M. Hankiewicz, P. Recher, B. Trauzettel, S.C. Zhang, L.W. Molenkamp. Nature Physics, **7**, 418 (2011).
[30] D.A. Kozlov, Z.D. Kvon, N.N. Mikhailov, S.A. Dvoretskii. JETP Lett., **96**, 730 (2012).
[31] G.M. Gusev, D.A. Kozlov, A.D. Levin, Z.D. Kvon, N.N. Mikhailov, S.A. Dvoretsky. Phys. Rev. B, **96**, 045304 (2017).
[32] G.M. Gusev, E.B. Olshanetsky, Z.D. Kvon, N.N. Mikhailov. Sol. St. Commun., **302**, 113701, (2019).
[33] Chen-Hsuan Hsu, Peter Stano, Jelena Klinovaja, Daniel Loss. Semicond. Sci. Technol., **36**, 123003 (2021).
[34] G.M. Minkov, A.V. Germanenko, I.V. Gornyi. Phys. Rev. B, **70**, 245423 (2004).
[35] L. Altshuler, A.G. Aronov, A.I. Larkin, D.E. Khmelnitskii. Zh. Eksp. Teor. Fiz., **54**, 411 (1981).
[36] O.E. Raichev, P. Vasilopoulos. J. Phys.: Condens. Matter, **12**, 589 (2000).
[37] I.S. Burmistrov, I.V. Gornyi, K.S. Tikhonov. Phys. Rev. B, **84**, 075338 (2011).
[38] I.R. Pagnossin, A.K. Meikap, T.E. Lamas, G.M. Gusev, J.C. Portal. Phys. Rev. B, **78**, 115311 (2008).
[39] G.M. Minkov, A.V. Germanenko, O.E. Rut, A.A. Sherstobitov, A.K. Bakarov, D.V. Dmitriev. Phys. Rev. B, **82**, 165325 (2010).
[40] B.L. Altshuler, A.G. Aronov, D.E. Khmelnitsky. J. Phys. C, **15**, 7367 (1982).
[41] V. Krueckl, K. Richter. Semicond. Sci. Technol., **27**, 124006 (2012).

Translated by T.Zorina